Report no. 99/19

Adaptive Finite Element Simulation of Steady State Currents at Microdisc Electrodes to a Guaranteed Accuracy.

Kathryn Harriman David Gavaghan Paul Houston Endre Süli

We consider the general problem of numerical simulation of the currents at microelectrodes using an adaptive finite element approach. Microelectrodes typically consist of an electrode embedded (or recessed) in an insulating material. For all such electrodes, numerical simulation is made difficult by the presence of a boundary singularity at the electrode edge (where the electrode meets the insulator), manifested by the large increase in the current density at this point, often referred to as the "edge-effect". Our approach to overcoming this problem involves the derivation of an *a posteriori* bound on the error in the numerical approximation for the current which can be used to drive an adaptive mesh-generation algorithm. This allows us to calculate the current to within a *prescribed* tolerance. Here we demonstrate the power of the method for a simple model problem — an E reaction mechanism at a microdisc electrode — for which the analytical solution is known, then we extend the work to the case of a (pseudo) first order EC′ reaction mechanism at both an inlaid and a recessed disc.

Oxford University Computing Laboratory
Numerical Analysis Group
Wolfson Building
Parks Road
Oxford, England OX1 3QD

December, 1999

1 Introduction

Microelectrodes are widely used for a variety of electrochemical measurement techniques. Except for the simplest possible problem of steady-state diffusion to a microdisc, no simple analytical solution exists. As a result, the problem of solving the equations modelling mass transport of the electroactive species has attracted the interest of many workers using a variety of analytical and numerical simulation methods (see, for example, [25] and the references cited therein).

Numerical simulation at microelectrodes typically requires solution of reaction-diffusion or reaction-diffusion-convection equations in a two-dimensional domain. The most commonly used electrode geometry is the microdisc, where the working electrode consists of a cylindrical wire embedded in an insulator. An increasingly popular alternative is the channel electrode, in which the working electrode consists of a narrow rectangular strip, again embedded in an insulator [15]. Numerical simulation of diffusion processes at these types of electrodes is made difficult by the presence of boundary singularities where the working electrode meets the insulator, giving a discontinuity in the normal derivative of the solution for the concentration at such points. The presence of the singularity is manifested by a large increase in the current density at the electrode edge, which is often termed the "edge-effect". In an earlier paper, Gavaghan [25] gave a detailed description of the effect of such singularities on the numerical performance of standard numerical methods, showing that practical convergence rates were lower than the optimal rate achieved for the one-dimensional case, resulting in very inaccurate approximations for the quantity of interest, the current. He concluded that it is not possible to obtain values of the simulated current to the required accuracy using regular meshes within reasonable computing time.

1.1 Previous Work

Various numerical methods have been suggested in the electrochemical literature to attempt to overcome the problems caused by singularities, and these fall into four broad categories. The first of these is due to Heinze [31, 32] who considered both chronoamperometry [31] and sweep voltammetry [32], and used a special method of integration at the electrode edge to allow for the increased flux in this region, but made no attempt to correct the effect that the singularity has on the concentration values. The second approach, first used by Crank and Furzeland [16], and further developed by Gavaghan and Rollett [29], Galceran *et al.* [23] and Parkins [39], involves matching a locally valid series solution in the region of the singularity with the numerical solution sufficiently far from the singularity as to be comparatively unaffected by it. The third approach involves the use of coordinate transformations and can be further subdivided into the approach adopted by Taylor *et al.* [44] and that of Amatore and co-workers [4, 36, 37]. Taylor *et al.* [44] used a coordinate transformation which greatly increases the density of points in the neighbourhood of the singularity whilst Wightman & Amatore and co-workers [4, 36, 37] used a transformation based on the analytical solution of the steady-state problem, which essentially "folds" the radial axis at the electrode edge, effectively removing the

singularity. This latter approach has also been applied by Verbrugge and Baker [47], and further refined by Alden and Compton [2, 3]. Finally, Gavaghan [26, 27, 28] and Bartlett & Taylor [9] have used a mesh refinement approach based on an error-analysis which also increases the density of points in the vicinity of the singularity. A comprehensive review of both analytical and numerical work at microelectrodes has been given by Alden [1].

1.2 Difficulties with Previous Approaches

The main difficulty with all of the above approaches is the inability to demonstrate accuracy for a general electrochemical problem. All of the authors begin by solving for a steady-state E reaction mechanism at a disc electrode, since this is the only such problem for which a closed-form analytical solution exists [43]. For all other problems the authors have to rely on extending the results for the simple model problem to more complex problems, or on extensive convergence testing to demonstrate accuracy. The most comprehensive results for a wide range of reaction mechanisms and electrode geometries have been presented by Alden and Compton [3], and Alden [1]. These authors found that even employing coordinate transformations in order to demonstrate comprehensively that convergence had been achieved for a general steady state reaction mechanism (e.g. ECE or EC_2E) required a 50×50 up to a 50×400 mesh at disc electrodes [1], and typically a 2000×500 mesh for general reaction mechanisms at a channel electrode [1]; that is up to a million nodes. In addition, no generally applicable approach has yet been devised that can be applied to all reaction mechanisms and all commonly occurring microelectrode geometries.

1.3 Approach Taken in this Paper

In this paper we introduce an alternative approach, developed for the solution of complex physical problems [10, 11, 20, 21, 34] which we believe will form the basis for a general and comprehensive simulation method for electrochemical problems. The method is based on deriving an *a posteriori* error bound on the accuracy of the calculation of the current which can be used to drive a mesh-adaptation routine which gives an approximate value of the current to within a *guaranteed tolerance*. Since the adaptivity is guided by the error in the current, the meshes derived are near-optimal for the simulation of the current. Our method is based on the finite element technique and associated error analysis, and results in a completely automated solution procedure which is extraordinarily fast and efficient in terms of both CPU time and memory requirements. Here we introduce the necessary theory and analysis for the simple model problem of the steady-state current for an E mechanism at a microdisc then we extend the application to a steady-state EC' mechanism at inlaid and recessed discs.

2 The Model Problem

We consider the simple reaction mechanism

$$A \pm ne^- \quad = \quad B \tag{2.1}$$

at a disc electrode. Assuming that semi-infinite mass transport occurs, axial symmetry allows the steady-state diffusion equation to be written in cylindrical polar coordinates as

$$\frac{\partial^2 u}{\partial r^2} + \frac{1}{r}\frac{\partial u}{\partial r} + \frac{\partial^2 u}{\partial z^2} \quad = \quad 0 \quad . \tag{2.2}$$

Throughout this paper we will solve for the normalised concentration $u = c/c_0$ where c_0 is the bulk concentration of species A.

2.1 The Boundary Conditions

Assuming that the reaction is sufficiently rapid that the surface concentration is zero, the boundary conditions for the problem are

$$\begin{array}{rl} u = 0, & r \leq 1, z = 0, \\ \frac{\partial u}{\partial n} = 0, & r > 1, z = 0, \\ & r = 0, z \geq 0, \\ u = 1, & r, z \to \infty, \end{array} \tag{2.3}$$

where we have taken the electrode radius to be 1 by normalising the spatial coordinates.

The form of the boundary conditions on $z = 0$ gives a boundary singularity at $(1, 0)$ (since $\partial u/\partial r$ is discontinuous there), which would cause problems for standard numerical techniques as described above.

2.2 The Current

We shall calculate the dimensionless current to the electrode which is given by

$$I \quad = \quad \frac{\pi}{2}\int_0^1 \left(\frac{\partial u}{\partial z}\right)_{z=0} r dr \quad . \tag{2.4}$$

2.3 The Exact Solution

The exact solution to the steady state problem was given by Saito [43] as

$$u \quad = \quad 1 - \frac{2}{\pi}\int_0^\infty \frac{\sin m}{m} J_0(rm) e^{-zm} dm \quad , \tag{2.5}$$

where J_0 is the zeroth order Bessel function. Differentiating with respect to z and setting $z = 0$ gives

$$\left(\frac{\partial u}{\partial z}\right)_{z=0} \quad = \quad \frac{2}{\pi}\int_0^\infty \sin m \, J_0(rm) \, dm \tag{2.6}$$

and using standard integration results (see for example [30]) we see this is equivalent to

$$\left(\frac{\partial u}{\partial z}\right)_{z=0} = \frac{2}{\pi}\frac{1}{\sqrt{1-r^2}} \ . \tag{2.7}$$

Hence integrating Eq. (2.7) over the electrode surface yields a non-dimensional current of $I = 1$.

Crank and Furzeland [16] rewrote Saito's solution in the more convenient form

$$u = \begin{cases} 1 - \frac{2}{\pi}\sin^{-1}\left\{\frac{2}{\sqrt{z^2+(1+r)^2}+\sqrt{z^2+(1-r)^2}}\right\} \ , & z > 0, \\ 0 \ , & 0 \le r \le 1, \ z = 0, \\ 1 - \frac{2}{\pi}\sin^{-1}\left\{\frac{1}{r}\right\} \ , & r > 1, \ z = 0. \end{cases} \tag{2.8}$$

To test our numerical method we shall solve the problem in the region $[0, r_{\max}] \times [0, z_{\max}]$. We shall then use the exact solution as given by Crank and Furzeland as the boundary condition on $r = r_{\max}$ and $z = z_{\max}$.

Remark Numerically we can only solve the model problem in a finite domain. Since we are interested in the efficacy of our method in overcoming the problems caused by the boundary singularity, it is legitimate to replace the conditions at infinity by the exact values at a finite distance from the electrode surface.

3 Numerical Techniques

Our numerical technique is based on the finite element method. Our primary interest is in calculating an estimate of the current, I_{est} say, to within some given tolerance, so we require methods of estimating the *error*. If the exact value of the current is denoted by I, then standard theoretical bounds on the error $|I - I_{est}|$ can be derived without first finding I_{est}. These are known as *a priori* error bounds and indicate the expected order of convergence of the solution. However these bounds are usually of the form $|I - I_{est}| \le Ch^k$ where h is the mesh size and C is some constant, dependent on the exact solution of the partial differential equation, and k depends on both the degree of the approximating polynomial and the regularity of the true solution u to the PDE[1]. Such bounds are useful in that they show the rate at which the method converges as $h \to 0$, however, in general the size of the constant C is not known, and hence the bound is not computable. Of much greater use are *a posteriori* error bounds, which can be expressed in terms of the finite element solution u^h in such a way that they are exactly computable. Our methods are based on deriving an *a posteriori* error bound which will form the basis of an adaptive finite element computation.

In general an adaptive mesh refinement strategy should be based on rigorous *a posteriori* error bounds in order to ensure that the quantity of interest, e.g. the solution

[1] We show later that the basic finite element method using piecewise linear finite elements on triangles gives convergence which is approximately $Ch^{1/2}$, on a regular mesh, which is extremely slow.

or a linear functional of the solution, is both reliably and efficiently computed. In this paper, we shall derive an *a posteriori* bound for the error in the computed current along the electrode surface; the resulting bound will be implemented into an adaptive finite element algorithm to ensure that the current is computed to within a user–defined error tolerance with the minimum amount of computational effort. The proof of this error bound will be based on a duality argument which uses a *dual* or *adjoint* problem. Based on this dual problem, we then derive a bound on the error in the computed current in terms of the finite element residual and the dual solution. We note that the residual measures the extent to which the computed numerical solution u^h fails to satisfy the underlying partial differential equation. The presence of the dual solution in the resulting error bound provides important local information regarding the sensitivity of the relevant error quantity $J(\cdot)$ (e.g. the current) with respect to variations in the local mesh size. Indeed, it has been clearly demonstrated that if the dual solution is omitted from the error estimate and mesh refinement is guided by the local size of the residual, then the resulting adaptive mesh refinement algorithm may produce a sequence of finite element meshes on which the computed error quantity $J(u^h)$ may *not* converge to the true value $J(u)$, cf. [34], for example. In general, the analytical solution to the dual problem is not known, and must therefore be numerically approximated as part of the adaptive mesh refinement algorithm. In this case the reliability of the *a posteriori* error bound can no longer be guaranteed; the degree of confidence that the user may have in the error bound will very much depend on how much computational work he is willing to invest into computing the dual solution. Not withstanding this, the approach adopted in this paper has been successfully applied to both linear and nonlinear partial differential equation models in a wide range of physical applications, see [10, 11, 38], for example.

3.1 The Finite Element Method

As indicated earlier, we shall test our numerical method on the finite domain shown in Figure 1. The boundary conditions on $\partial\Omega_1$, $\partial\Omega_2$ and $\partial\Omega_5$ will be the same as those in Eq. (2.3) and we shall use Eq. (2.8) to define Dirichlet boundary conditions on $\partial\Omega_3$ and $\partial\Omega_4$. We define $\partial\Omega_D$ to be the part of the boundary where Dirichlet boundary conditions are specified and $\partial\Omega_N$ to be the part where there are Neumann boundary conditions; hence $\partial\Omega_D = \partial\Omega_1 \cup \partial\Omega_3 \cup \partial\Omega_4$ and $\partial\Omega_N = \partial\Omega_2 \cup \partial\Omega_5$.

In the finite element method we require the analytical solution u of the problem to lie in the Sobolev space $H^1(\Omega)$. In cylindrical polar coordinates, Sobolev spaces become weighted inner product spaces so that $H^1(\Omega)$ is defined by

$$H^1(\Omega) \;=\; \left\{ u : \int_\Omega \left[u^2 + \left(\frac{\partial u}{\partial r}\right)^2 + \left(\frac{\partial u}{\partial z}\right)^2 \right] r dr dz < \infty \right\} \;; \qquad (3.1)$$

that is the space of functions such that the function itself, and its first derivatives are square integrable on the computational domain Ω with respect to $rdrdz$. We may then

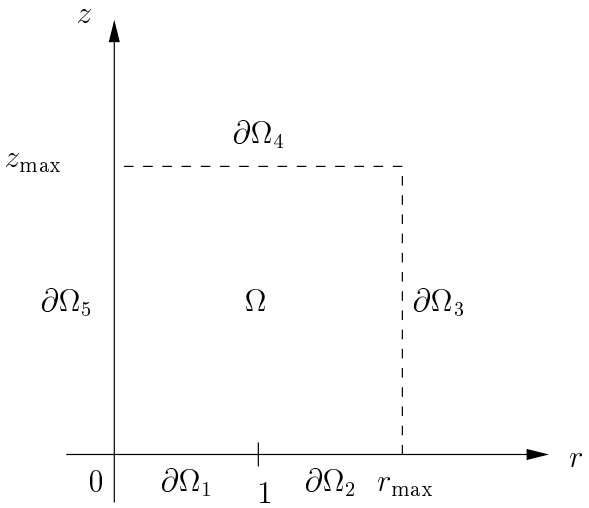

Figure 1: The five parts of the boundary.

define the corresponding spaces $H^1_E(\Omega)$ and $H^1_{E_0}(\Omega)$ by

$$H^1_E(\Omega) = \left\{u \in H^1(\Omega) : u \text{ satisfies Dirichlet boundary conditions on } \partial\Omega_D\right\} , \quad (3.2)$$
$$H^1_{E_0}(\Omega) = \left\{u \in H^1(\Omega) : u = 0 \text{ on } \partial\Omega_D\right\} . \quad (3.3)$$

For the disc electrode problem the weak formulation of the boundary value problem requires us to find $u \in H^1_E(\Omega)$ such that

$$\int_\Omega \nabla u \cdot \nabla v r dr dz = 0 \qquad \forall v \in H^1_{E_0}(\Omega) , \quad (3.4)$$

cf. Appendix A of [23].

The standard technique for evaluating the current would be to substitute the approximate solution (or some interpolant of that solution) into Eq. (2.4) and evaluate the integral. However, a more accurate method can be derived: to this end we first define ψ to be any function which satisfies

$$\psi = \begin{cases} 1 & \text{on } \partial\Omega_1 , \\ 0 & \text{on } \partial\Omega_3 \cup \partial\Omega_4 . \end{cases} \quad (3.5)$$

We then let $H^1_\psi(\Omega)$ be the space of functions in $H^1(\Omega)$ that are equal to ψ on $\partial\Omega_D$. For $v \in H^1_\psi(\Omega)$, we have

$$\int_\Omega \nabla^2 u v r dr dz = 0 . \quad (3.6)$$

Applying Green's theorem gives

$$\int_\Omega \nabla u \cdot \nabla v r dr dz - \int_{\partial\Omega} v \frac{\partial u}{\partial n} r ds = 0 , \quad (3.7)$$

and hence

$$\int_\Omega \nabla u \cdot \nabla v r dr dz + \int_0^1 \frac{\partial u}{\partial z} r dr \;=\; 0 \;\;, \tag{3.8}$$

since other contributions to the boundary integral are zero. We define $N_\psi(u)$ by

$$N_\psi(u) \;=\; -\frac{\pi}{2}\int_\Omega \nabla u \cdot \nabla v r dr dz \;=\; B(u,v) \;\;, \qquad v \in H^1_\psi(\Omega) \;\;, \tag{3.9}$$

and we shall use this expression to evaluate the current instead of Eq. (2.4). Note that on the continuous level the definitions Eq. (2.4) and Eq. (3.9) of the current are identical. It is also important to note that the latter definition of the current Eq. (3.9) is independent of the choice of v, provided $v \in H^1_\psi(\Omega)$. Below we shall demonstrate that numerical approximations to the current based on Eq. (3.9) are substantially more accurate than those that use Eq. (2.4).

The idea of expressing the current as an integral over the entire domain rather than evaluating it directly by inserting the finite element solution into Eq. (2.4) was developed by Babuška and Miller [5, 6, 7]. They refer to it as the *extraction method* and, in a series of papers [5, 6, 7], they use it to calculate displacements and stresses in structural mechanics.

3.2 The Finite Element Formulation of the Problem

We split the domain Ω into triangles of maximum edge-length h and we define S^h_E, $S^h_{E_0}$ and S^h_ψ to be finite-dimensional subspaces of $H^1_E(\Omega)$, $H^1_{E_0}(\Omega)$ and $H^1_\psi(\Omega)$, respectively, consisting of continuous functions which are polynomials of degree p in each triangle. Then the finite element formulation of the problem Eq. (3.4) is to find $u^h \in S^h_E$ such that

$$\int_\Omega \nabla u^h \cdot \nabla v^h r dr dz \;=\; 0 \qquad \forall v^h \in S^h_{E_0} \tag{3.10}$$

and we approximate the current $I = N_\psi(u)$ using

$$N_\psi(u^h) \;=\; -\frac{\pi}{2}\int_\Omega \nabla u^h \cdot \nabla v^h r dr dz \;=\; B(u^h, v^h) \;\;, \qquad v^h \in S^h_\psi \;\;. \tag{3.11}$$

It can now be seen that on the discrete level the approximation of the current obtained by replacing u by u^h in Eq. (2.4) and the new definition $N_\psi(u^h)$ are different. We note that the definition Eq. (3.11) of $N_\psi(u^h)$ is independent of the choice of $v^h \in S^h_\psi$. We shall choose to approximate the current using Eq. (3.11); we shall see later that this definition has a faster rate of convergence to the exact value of the current as the computational mesh is refined than using Eq. (2.4) with u replaced by u^h which is the standard method in electrochemistry.

3.3 The Dual Problem

We have already stated that the definition of $N_\psi(u^h)$ is independent of the choice of $v^h \in S^h_\psi$. In fact we shall choose v^h to be the finite element approximation to the solution of the dual problem which can be defined weakly in terms of the bilinear form $B(\cdot,\cdot)$: find $w \in H^1_\psi(\Omega)$ such that

$$B(\phi, w) = 0 \qquad \forall \phi \in H^1_{E_0}(\Omega) \ . \tag{3.12}$$

From Eq. (3.9) we see that, for this particular problem, the weak formulation of the dual is to find $w \in H^1_\psi(\Omega)$ such that

$$\int_\Omega \nabla w \cdot \nabla \phi r dr dz = 0 \qquad \forall \phi \in H^1_{E_0}(\Omega) \ . \tag{3.13}$$

Application of Green's theorem to Eq. (3.13) yields the strong formulation of the dual problem:

$$\frac{\partial^2 w}{\partial r^2} + \frac{1}{r}\frac{\partial w}{\partial r} + \frac{\partial^2 w}{\partial z^2} = 0 \ , \tag{3.14}$$

with boundary conditions

$$\begin{array}{rl} w = 1, & r \le 1, z = 0, \\ \frac{\partial w}{\partial n} = 0, & r > 1, z = 0, \\ & r = 0, z \ge 0, \\ w = 0, & r = r_{\max}, z > 0, \\ & r > 0, z = z_{\max}. \end{array} \tag{3.15}$$

So the boundary conditions on $z = 0$ indicate that w has a similar boundary singularity to u.

We note that Eq. (3.12) holds for all $\phi \in H^1_{E_0}(\Omega)$; in particular we may take $\phi = u - u^h$ to give

$$B(u - u^h, w) = 0 \ . \tag{3.16}$$

This fundamental property of the dual problem forms the basis of the duality argument which will be the key to our error analysis.

3.4 Solution of the Finite Element Problems

We choose to solve the finite element problem Eq. (3.10) using continuous piecewise linear finite elements on triangular meshes. We use the same mesh for the dual problem but approximate the solution using continuous piecewise quadratic finite elements; the reason for this choice is explained at the end of the *a posteriori* error analysis in the Appendix. More details of the application of the finite element method can be found in [35, 42].

4 An Adaptive Finite Element Solution

In this section we describe the adaptive finite element algorithm which we use to calculate the current to within a user-supplied tolerance in an automated manner. The key ingredient of the algorithm is an *a posteriori* bound on the error between the analytical value of the current and its finite element approximation $N_\psi(u^h)$.

First we state the *a posteriori* error bound for the problem; the proof of this is derived in the Appendix.

4.1 An *A Posteriori* Error Bound

Let h_α be the length of the longest side of triangle α and let c_1 be a constant satisfying

$$c_1 h_\alpha^2 \;\leq\; area(\alpha) \tag{4.1}$$

where $area(\alpha)$ is the area of triangle α. Also let J_α be the transformation matrix for each triangle α in the triangulation of the computational domain Ω, defined by

$$J_\alpha \;=\; \begin{pmatrix} r_2 - r_1 & r_3 - r_1 \\ z_2 - z_1 & z_3 - z_1 \end{pmatrix} \;, \tag{4.2}$$

where (r_i, z_i), $i = 1, \ldots, 3$, denote the vertices of element α. Then we have the *a posteriori* error bound

$$|N_\psi(u) - N_\psi(u^h)| \;\leq\; \sum_\alpha \epsilon_\alpha \;\equiv\; \epsilon \;, \tag{4.3}$$

where

$$\begin{aligned} \epsilon_\alpha \;=\; & \frac{9^{1/4}\pi}{32^{1/4}} \parallel [\partial u^h/\partial n] \parallel_{L_2(\partial\alpha)} \frac{\parallel J_\alpha \parallel_2^{1/2}}{h_\alpha c_1^{1/2}} \parallel v^h - w \parallel_{L_2(\alpha)}^{1/2} \\ & \times \left(\parallel v^h - w \parallel_{L_2(\alpha)} + \parallel J_\alpha^T \parallel_2 \parallel \nabla(v^h - w) \parallel_{L_2(\alpha)} \right)^{1/2} \;. \end{aligned} \tag{4.4}$$

The L_2 norm in this expression is defined by

$$\parallel w \parallel_{L_2(\alpha)} \;=\; \left(\int_\alpha |w|^2 r dr dz \right)^{1/2} \;. \tag{4.5}$$

Finally, note that the 2-norm of a matrix, J_α, is defined by

$$\parallel J_\alpha \parallel_2 \;=\; \sup_{\mathbf{x} \neq 0} \frac{\parallel J_\alpha \mathbf{x} \parallel_2}{\parallel \mathbf{x} \parallel_2} \;, \tag{4.6}$$

where

$$\parallel \mathbf{x} \parallel_2 \;=\; \left(\mathbf{x}^T \mathbf{x} \right)^{1/2} \;. \tag{4.7}$$

It can be shown that

$$\parallel J_\alpha \parallel_2 \;=\; \max_i \sigma_i \;, \tag{4.8}$$

where σ_i^2 are the eigenvalues of $J_\alpha^T J_\alpha$ (see [19]).

4.2 The Adaptive Algorithm

We are now in a position to define an adaptive algorithm as follows: Let TOL be the prescribed tolerance;

1. Choose an initial coarse mesh $\mathcal{K}^0$;

2. Calculate the finite element solution on the ith mesh $\mathcal{K}^i$, $i \geq 0$;

3. Calculate the *a posteriori* error bound ϵ^i on the mesh $\mathcal{K}^i$.

   If $\epsilon^i < TOL$ then **STOP**, the solution is accurate to within the prescribed tolerance;

4. Otherwise refine the mesh, increase i by 1, and go to step 2.

We have already discussed in detail the finite element solution and the calculation of the *a posteriori* error bound, now we discuss the method of mesh adaptation.

4.3 Mesh Refinement

The form of the *a posteriori* error bound is

$$|N_\psi(u) - N_\psi(u^h)| \;\leq\; \epsilon \;\equiv\; \sum_\alpha \epsilon_\alpha \tag{4.9}$$

and this suggests equidistribution of ϵ over the triangles. To do so, we adopt the red-green isotropic refinement strategy of Bank (see [8]) in which we evaluate ϵ_α, the contribution to the *a posteriori* error bound from triangle α, and if

$$\epsilon_\alpha \;\geq\; \frac{TOL}{n_tri} \;, \tag{4.10}$$

(where n_tri is the number of triangles in the mesh) we label triangle α as red. We refine a red triangle by joining the midpoints of the sides to get four similar triangles referred to as the children of the original triangle or parent, see Figure 2. After all these red refinements have been performed, further refinement is needed to remove all the hanging nodes. If a triangle has two or three hanging nodes it is red refined. When all red refinements are completed all triangles with one hanging node are labelled green and are refined by joining the hanging node to the opposite vertex, see Figure 3. Green refinement is only temporary and is removed before the next stage of refinement in order to prevent unnecessarily long and thin triangles. Re-coarsening is also possible, if each of the errors in the four children is less than a certain tolerance, related to the original tolerance, we remove the red refinement. Once the adaptive tolerance has been specified, all the refinement is done automatically.

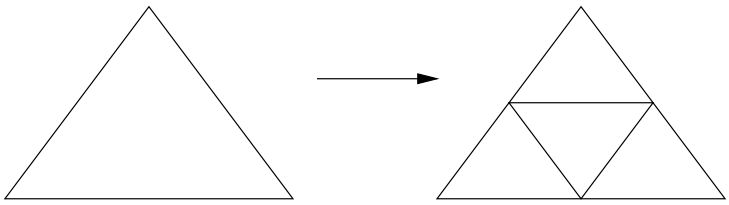

Figure 2: A red refinement.

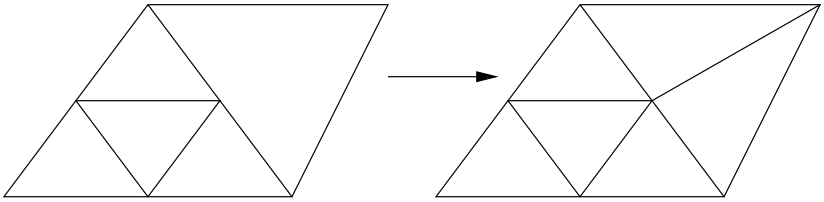

Figure 3: A green refinement to remove a hanging node.

5 Results

We choose $TOL = 0.05$ so that we are guaranteed 5% accuracy in the current. In fact, in practice we will get even greater accuracy than this as the *a posteriori* error bound overestimates the error by a factor of about 10. Hence we perform a red refinement on triangle α if

$$\epsilon_\alpha \geq \frac{0.05}{n_tri} \tag{5.1}$$

and we re-coarsen if

$$\epsilon_{\alpha_i} < \frac{0.05}{10 n_tri} \tag{5.2}$$

where α_i are the children of triangle α. The choice of the factor relating the tolerance for re-coarsening to the original tolerance is somewhat arbitrary. The factor needs to satisfy two competing criteria. It must be small enough that triangles re-coarsened at one stage are not refined at the next, but equally it must be large enough to actually allow some re-coarsening. Poor balance between these two factors will still lead to accurate values of the current, but the algorithm will be less efficient. After performing numerical experiments with different values of the factor, we chose 1/10: with a smaller factor more nodes were required for the tolerance to be achieved, whilst with a larger factor more refinement stages were needed, suggesting that we have found a reasonable balance between the two criteria.

We take $r_{\max} = z_{\max} = 2$ and we choose to begin with a regular mesh with 32 triangles. In Table 1 we show the numbers of triangles (n_tri), the number of nodes (n_nods), currents and error estimates on the resulting sequence of triangulations. The effectivity index is also shown; this is defined to be the estimated error divided by the actual error, so it measures the sharpness of the error bound. Ideally the index should

be as near to one as possible (though of course always greater than 1). The effectivity index is computable in this case since we know the exact value of the current; normally however we will not know the exact solution and this index will not be available to us. It should be noted that the effectivity index can be reduced by estimating the constant in the trace inequality numerically (see Eq. (A.24) below). The size of the constant used in Eq. (A.24) reflects the fact that the inequality is valid for any function in $H^1(\alpha)$ but the inequality need not necessarily be sharp for a specific function under consideration. Indeed, using a numerical estimate of the trace constant can decrease the effectivity index by a factor of up to 4, see [33]. The accuracy that we are able to obtain on the sixth mesh is truly remarkable — the calculation of the current is accurate to 0.25% using only 396 unknowns. The total CPU time for calculations on all 6 meshes was just 1.63 seconds.

mesh	*n_tri*	*n_nods*	estimated current	actual error	estimated error	effectivity index
1	32	25	1.081997	8.1997×10^{-2}	0.828703	10.11
2	94	59	1.039599	3.9599×10^{-2}	0.412515	10.42
3	201	116	1.019756	1.9756×10^{-2}	0.214510	10.85
4	372	208	1.009729	9.729×10^{-3}	0.114844	11.80
5	527	301	1.005197	5.197×10^{-3}	6.88761×10^{-2}	13.25
6	720	396	1.002543	2.543×10^{-3}	4.20017×10^{-2}	16.52

Table 1: The triangulations produced by the adaptive finite element method for the steady state disc electrode problem.

The actual meshes generated by the automatic procedure are shown in Figure 4. We see from the second mesh that at the first refinement level most of the triangles are red-refined though some green refinement can be seen to remove hanging nodes, notably in the bottom left-hand corner. At the next stage the mesh begins to look as we expect, triangles are added near the boundary singularity but the mesh remains fairly coarse further away. The process continues until we reach the sixth and final mesh at which point the *a posteriori* error bound is less than the preset tolerance TOL so the algorithm terminates. The final mesh has very small triangles near to the boundary singularity and looks very much as we would have anticipated.

5.1 Comparison with Regular Meshes

Here we illustrate briefly that our adaptive finite element method is effective by considering the extra work needed if a simple regular mesh were to be used instead. Also we show that using the approximation $N_\psi(u^h)$, cf. Eq. (3.11), for the current is the most efficient.

First we use a regular mesh and approximate the current using $N_\psi(u^h)$: halving the mesh spacing approximately halves the error in the current (see Table 2), suggesting that the error in the current is order $O(h)$. This is backed up by the *a priori* error

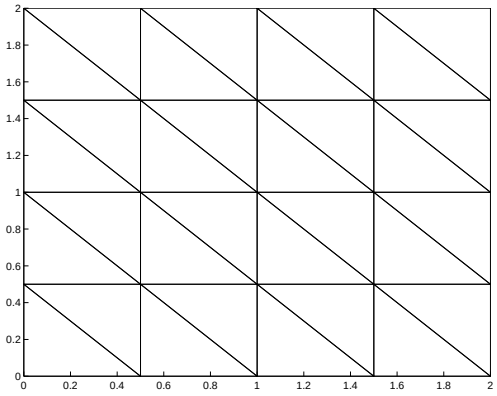

(a) 1st mesh, 25 nodes, 32 triangles

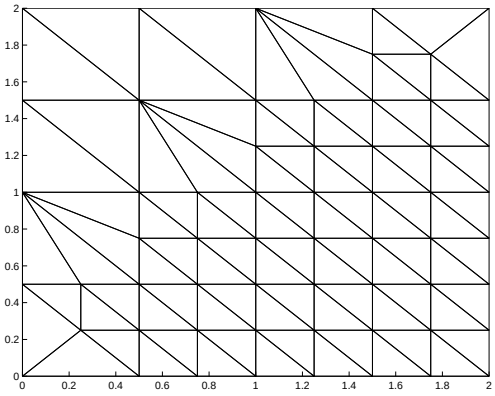

(b) 2nd mesh, 59 nodes, 94 triangles

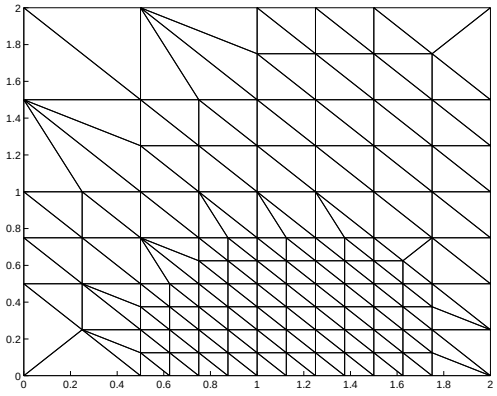

(c) 3rd mesh, 116 nodes, 201 triangles

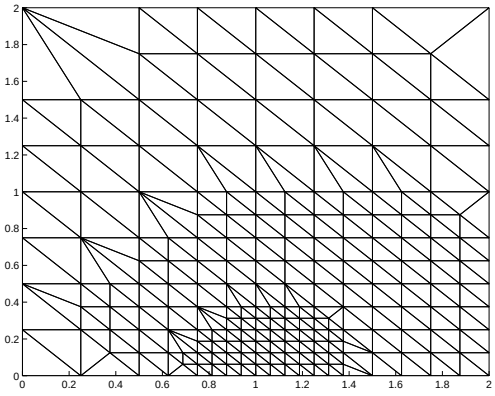

(d) 4th mesh, 208 nodes, 372 triangles

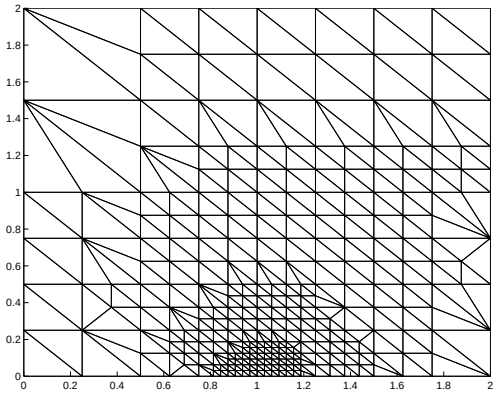

(e) 5th mesh, 301 nodes, 527 triangles

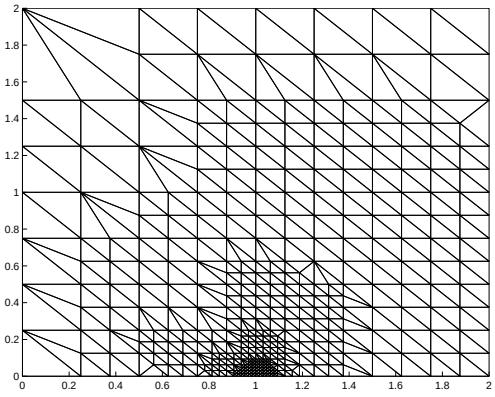

(f) 6th mesh, 396 nodes, 720 triangles

Figure 4: The meshes produced by an adaptive finite element method for the steady state disc electrode problem.

bound derived in the Appendix. To achieve the same accuracy as with the adaptive algorithm (that is, an error of 2.5×10^{-3}) we would require 123 mesh spacings in each direction, a total of 15376 nodes altogether. This took 218.2 seconds of CPU time, two orders of magnitude longer than was needed for the adaptive finite element solution.

N	current	|error|	order
4	1.081998	0.081998	
8	1.039473	0.039473	1.05
16	1.019368	0.019368	1.03
32	1.009594	0.009594	1.01
64	1.004774	0.004774	1.01

Table 2: Values of the numerical approximation $N_\psi(u^h)$ to the current $N_\psi(u)$ and the error $N_\psi(u) - N_\psi(u^h)$ evaluated on a regular mesh with N mesh spacings in each direction.

Secondly, we consider approximating the current using the expression

$$\frac{\pi}{2} \int_0^1 \left(\frac{\partial u^h}{\partial z} \right)_{z=0} r dr \tag{5.3}$$

instead of Eq. (3.11). Here we have simply inserted the numerical solution u^h into the original definition of the current Eq. (2.4); this is the standard method used in electrochemistry. Since u^h is piecewise linear, its partial derivatives are constant on each triangle in the triangulation of Ω so this expression for the current can be evaluated easily. From Table 3 we see that this approximation converges to $N_\psi(u)$ at less than half the rate of $N_\psi(u^h)$; estimating the error between Eq. (5.3) and the exact value of the current to be $O(h^{0.4})$ means that we would require over 1.5×10^{13} nodes using Eq. (5.3) to achieve the same accuracy as the sixth adaptive mesh gave with only 396 nodes using Eq. (3.11).

N	current	|error|	order
4	0.451060	0.548940	
8	0.551208	0.448792	0.29
16	0.643869	0.356131	0.33
32	0.725287	0.274123	0.38
64	0.792848	0.207152	0.40

Table 3: Values of the current evaluated using the expression Eq. (5.3), the associated error, and its order of convergence on a sequence of regular meshes with N mesh spacings in each direction.

From this we conclude that it is better to estimate the current using the expression $N_\psi(u^h)$ defined by Eq. (3.11) and that using an adaptive algorithm is the most efficient way to solve such a problem.

6 The EC′ Reaction Mechanism

The simulation algorithm described above will only be of value if it can also be shown to work for problems of practical interest to experimental electrochemists. One such steady-state problem which has aroused much interest in the electrochemical literature is the problem of an EC′ reaction mechanism at both an inlaid and a recessed disc [18, 24, 36, 40, 41]. Much of the recent interest in recessed microelectrodes is due to the rapid growth in the use of photolithographic techniques in the manufacture of microelectrode arrays [9]. As we show, the power of our new technique is made particularly clear for the case of the EC′ reaction mechanism at a recessed disc, and for both recessed and inlaid problems we are able to demonstrate remarkably good agreement with the recent analytical solutions on meshes which require at least an order of magnitude fewer nodes than previously described numerical solutions to these problems [9, 22].

7 Theory

We consider the problem of a steady state first-order EC′ reaction at an inlaid or recessed microdisc electrode whose geometry is as shown in Figure 5 (the particular case of the inlaid electrode is given by setting $L = 0$).

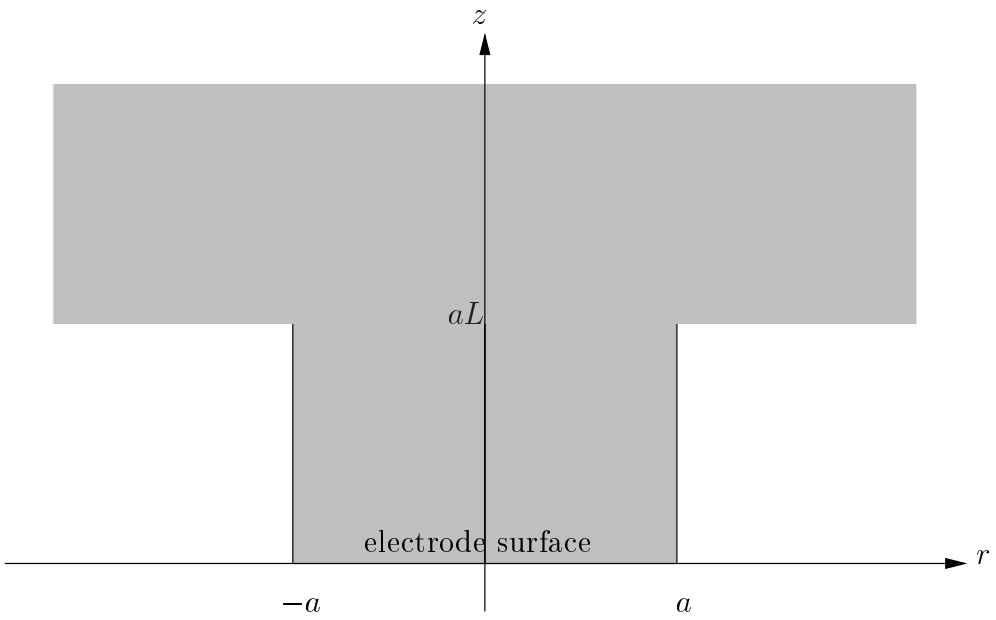

Figure 5: The geometry of a recessed microdisc electrode.

In the case of S being present in a large excess, pseudo-first order kinetics are achieved [18, 24, 41], and the EC′ mechanism is described by

$$\begin{aligned} A \pm ne^- &\rightarrow B \ , \\ B + S &\xrightarrow{k} A + Y \ , \end{aligned} \tag{7.1}$$

where k is the pseudo first-order reaction rate, n is the number of electrons involved, and S and Y are electro-inactive species. The steady-state transport equations for species A and B are then given by

$$\frac{\partial c_A}{\partial t} = D_A \nabla^2 c_A + k c_B = 0 \quad , \tag{7.2}$$

$$\frac{\partial c_B}{\partial t} = D_B \nabla^2 c_B - k c_B = 0 \quad , \tag{7.3}$$

where D_A and D_B are the diffusion coefficients and c_A and c_B are the concentrations of A and B, respectively.

Following the notation used by Galceran *et al.* [24], the boundary conditions on the electrode surface are given by

$$D_A \left(\frac{\partial c_A}{\partial z} \right)_{z=0} = -D_B \left(\frac{\partial c_B}{\partial z} \right)_{z=0} \quad , \tag{7.4}$$

$$\frac{c_B^s}{c_A^s} = \exp \left\{ \pm \frac{nF}{RT} (E - E^{0'}) \right\} = \delta \quad , \tag{7.5}$$

and $c_B \to 0$ and $c_A \to c_A^*$ as $r, z \to \infty$. Here, c_A^s and c_B^s denote the concentrations of A and B, respectively, on the electrode surface, F is Faraday's constant, R is the molar gas constant, T is the absolute temperature and $E^{0'}$ is the formal potential.

As in [41] and [24] a dimensionless concentration u can be introduced:

$$u = \frac{c_B}{c_B^s} = \frac{(D_A + \delta D_B) c_B}{\delta D_A c_A^*} \quad . \tag{7.6}$$

We take the electrode radius to be one by normalising the spatial coordinates. Thus u satisfies the equation

$$-\nabla^2 u + K u = 0 \quad , \tag{7.7}$$

where

$$K = \frac{k a^2}{D_B} \tag{7.8}$$

is the dimensionless reaction rate, and a is the actual electrode radius as shown in Figure 5. The boundary conditions are given by

$$\begin{array}{ll} u = 1, & r \le 1,\ z = 0, \\ u \to 0, & r, z \to \infty, \\ \frac{\partial u}{\partial n} = 0, & r = 0,\ z > 0, \\ & r = 1,\ 0 \le z \le L, \\ & r > 1,\ z = L, \end{array} \tag{7.9}$$

and the normalised current is

$$I = -\frac{\pi}{2} \int_0^1 \left(\frac{\partial u}{\partial z} \right)_{z=0} r dr \quad . \tag{7.10}$$

8 Analytic Solutions

We give brief details below of some recently derived very accurate analytical results which we will use to evaluate the accuracy of our numerical simulations.

8.1 The Inlaid Microdisc Electrode

Galceran *et al.* [24] have derived exact analytical solutions to the inlaid microdisc problem using Tranter's method [45, 46]. This method results in the system of linear equations for unknown coefficients a_m

$$\sum_{m=0}^{\infty} \Omega_{m,0} a_m = \sqrt{\frac{2}{\pi}} \ , \tag{8.1}$$

$$\sum_{m=0}^{\infty} \Omega_{m,n} a_m = 0 \ , \qquad (n > 0) \ , \tag{8.2}$$

where

$$\Omega_{m,n} = \int_0^{\infty} \frac{J_{2m+1/2}(\lambda) J_{2n+1/2}(\lambda)}{\sqrt{\lambda^2 + K}} d\lambda \ . \tag{8.3}$$

Here $J_k(\lambda)$ denotes a Bessel function of order k. The dimensionless current is then found to be

$$I = \sqrt{\frac{\pi}{2}} a_0 \ . \tag{8.4}$$

Although Eq. (8.4) is exact, in practice all the infinite sums must be truncated when computing the current, hence the accuracy depends on where we truncate these sums. More details of this are given in [24]. It is also noted that as K increases it becomes more difficult to compute the integrals in Eq. (8.3). For $K > 100$ it is suggested that one resorts to the asymptotic expression given by Phillips [40]:

$$I = \frac{\pi}{4} \left(\sqrt{K} + 1 + \frac{1}{4\sqrt{K}} \right) \ . \tag{8.5}$$

For $K > 10$, Eq. (8.5) is accurate to within 0.27%. Alternatively, one can use the Padé approximant derived by Rajendran and Sangaranarayanan [41]:

$$I = \frac{1 + 2.0016K^{1/2} + 1.8235K + 0.96367K^{3/2} + 0.307949K^2 + 0.049925K^{5/2}}{1 + 1.3650K^{1/2} + 0.8826K + 0.32853K^{3/2} + 0.063566K^2} \ . \tag{8.6}$$

8.2 The Recessed Microdisc Electrode

Galceran *et al.* [24] have also presented the exact solution to recessed microdisc problem in the following form: let a_m be the solution of the infinite system of linear equations

$$\sum_{m=0}^{\infty}(\Omega_{m,0}+2S_{m,0})a_m = \sqrt{\frac{2}{\pi}}\frac{1}{\cosh(\sqrt{K}L)}-\frac{4\tanh(\sqrt{K}L)}{\pi\sqrt{K}}a_0 \ , \tag{8.7}$$

$$\sum_{m=0}^{\infty}(\Omega_{m,n}+2S_{m,n})a_m = 0 \ , \qquad (n>0) \ , \tag{8.8}$$

where

$$S_{m,n} = \sum_{s=1}^{\infty}\frac{\tanh(\sqrt{K+x_s^2}L)J_{2m+1/2}(x_s)J_{2n+1/2}(x_s)}{x_s\sqrt{K+x_s^2}J_0^2(x_s)} \ , \tag{8.9}$$

and x_s is the sth positive zero of $J_1(x)$ and $\Omega_{m,n}$ is defined by Eq.(8.3). Then the current is given by

$$I = \sqrt{\frac{\pi}{2}}\frac{a_0}{\cosh(\sqrt{K}L)}+\frac{\pi}{4}\sqrt{K}\tanh(\sqrt{K}L) \ . \tag{8.10}$$

As $L\to\infty$ we have

$$I \to \frac{\pi}{4}\sqrt{K} \tag{8.11}$$

which is the well known case corresponding to one-dimensional semi-infinite diffusion [17].

8.2.1 Approximate Analytic Solutions

Galceran *et al.* [24] also present two approximate analytic solutions. The first uses the method followed by Bond *et al.* [12] and assumes a uniform concentration across the mouth of the recess. This leads to the approximation

$$I \approx \frac{\pi}{4}\sqrt{K}\left\{\coth(\sqrt{K}L)- \frac{2\pi\sqrt{K}}{\pi\sqrt{K}\sinh(2\sqrt{K}L)+4(1+\frac{6\sqrt{K}}{\pi}+\frac{3\pi^3K}{2^6}+(\frac{\pi\sqrt{K}}{4})^3)^{\frac{1}{3}}(\cosh(2\sqrt{K}L)-1)}\right\} . \tag{8.12}$$

Again this behaves like Eq. (8.11) as $L\to\infty$.

A second approximation is

$$I = \frac{\pi}{4}\sqrt{K}\coth(\sqrt{K}(L+\zeta)) \ , \tag{8.13}$$

where ζ is estimated using the work of Brunn *et al.* [14] by

$$\zeta \approx \frac{\pi}{4}\left(1+\frac{1}{21.4479+0.2564\coth(0.3439L)}\right)\frac{1}{\left(1+0.8\sqrt{K}\right)^{3/4}} \ . \tag{8.14}$$

9 An Adaptive Finite Element Solution

The general approach that we adopt in our numerical simulations is described above. Again we split the boundary of the domain into two parts, $\partial\Omega_D$, the part where Dirichlet boundary conditions are prescribed, and $\partial\Omega_N$, the part where Neumann boundary conditions are prescribed. We then define the Sobolev spaces $H^1(\Omega)$, $H^1_E(\Omega)$ and $H^1_{E_0}(\Omega)$ by Eq. (3.1), Eq. (3.2) and Eq. (3.3), respectively, and $H^1_\psi(\Omega)$ by

$$H^1_\psi(\Omega) \;=\; \left\{u \in H^1(\Omega) : u = 0 \text{ on } \partial\Omega_D \text{ except on the electrode surface where } u = 1\right\}. \tag{9.1}$$

Note that for this particular problem the spaces $H^1_E(\Omega)$ and $H^1_\psi(\Omega)$ are identical.

9.1 The Weak Form of the Problem

The weak form of the problem for u is: find $u \in H^1_E(\Omega)$ such that

$$\int_\Omega (\nabla u \cdot \nabla v + Kuv)\, r dr dz \;=\; 0 \qquad \forall v \in H^1_{E_0}(\Omega) \;. \tag{9.2}$$

We use the method described above to derive the weak formulation of the current,

$$I \;=\; N_\psi(u) \;=\; B(u,v) \;=\; \frac{\pi}{2}\int_\Omega (\nabla u \cdot \nabla v + Kuv)\, r dr dz \qquad \forall v \in H^1_\psi(\Omega) \;. \tag{9.3}$$

Again we note that this definition is independent of the choice of v from the function space $H^1_\psi(\Omega)$.

9.2 The Finite Element Form of the Problem

Defining the finite element spaces S^h_E, $S^h_{E_0}$ and S^h_ψ to be finite dimensional subspaces of $H^1_E(\Omega)$, $H^1_{E_0}(\Omega)$ and $H^1_\psi(\Omega)$, respectively, containing functions which are continuous polynomials of degree p in each triangle, we see that the finite element formulation of the problem is to find $u^h \in S^h_E$ such that

$$\int_\Omega \left(\nabla u^h \cdot \nabla v^h + K u^h v^h\right) r dr dz \;=\; 0 \qquad \forall v^h \in S^h_{E_0} \;, \tag{9.4}$$

and we estimate the current using

$$N_\psi(u^h) \;=\; B(u^h, v^h) \;=\; \frac{\pi}{2}\int_\Omega \left(\nabla u^h \cdot \nabla v^h + K u^h v^h\right) r dr dz \qquad \forall v^h \in S^h_\psi \;. \tag{9.5}$$

9.3 The Dual Problem

As for the previous problem, we choose v in Eq. (9.3) to be the solution of a suitable dual problem which is to find $w \in H_\psi(\Omega)$ such that

$$B(\phi, w) \;=\; 0 \qquad \forall \phi \in H^1_{E_0}(\Omega) \;\; , \tag{9.6}$$

where the bilinear form $B(\cdot,\cdot)$ is defined by Eq. (9.3). From this we see that the weak form of the dual problem is to find $w \in H^1_\psi(\Omega)$ such that

$$\int_\Omega (\nabla w \cdot \nabla \phi + K w \phi)\, r dr dz \;=\; 0 \qquad \forall \phi \in H^1_{E_0}(\Omega) \;\; . \tag{9.7}$$

Comparing Eq. (9.7) with Eq. (9.2) we find that this problem is, in fact, self-dual; in other words the primal and dual problems are identical.

9.4 An *A Posteriori* Error Bound

The *a posteriori* error bound for this problem is

$$|N_\psi(u) - N_\psi(u^h)| \;\leq\; \sum_\alpha \epsilon_\alpha \;=\; \epsilon \tag{9.8}$$

where

$$\begin{aligned} \epsilon_\alpha \;=\; & \frac{9^{1/4}\pi}{32^{1/4}} \,\| \, [\partial u^h/\partial n] \, \|_{L_2(\partial\alpha)} \, \frac{\| \, J \, \|_2^{1/2}}{h_\alpha c_1^{1/2}} \, \| \, v^h - w \, \|^{1/2}_{L_2(\alpha)} \\ & \times \left(\| \, v^h - w \, \|_{L_2(\alpha)} + \| \, J^T \, \|_2 \| \, \nabla (v^h - w) \, \|_{L_2(\alpha)} \right)^{1/2} \\ + \;\; & \frac{\pi}{2} K \, \| \, u^h \, \|_{L_2(\alpha)} \| \, v^h - w \, \|_{L_2(\alpha)} \quad . \end{aligned} \tag{9.9}$$

The notation used here is the same as for the previous problem. We can now use the adaptive algorithm and refinement strategy outlined above to find the current to within any prescribed tolerance.

10 Results

10.1 The Inlaid Microdisc Electrode

We consider first the case of an inlaid microdisc electrode, that is the special case of $L = 0$. We compare our simulated results with the analytical values for $K = 1$, 10, 100 and 1000. The tolerance for the adaptive finite element approximation for each case is chosen to guarantee 1% accuracy in the estimated current. The final mesh for each of the four problems is shown in Figure 6 and these are as we might expect. For lower values of K diffusion dominates and the boundary singularity causes more of a problem when evaluating the current, consequently more nodes are needed near the point $(1, 0)$.

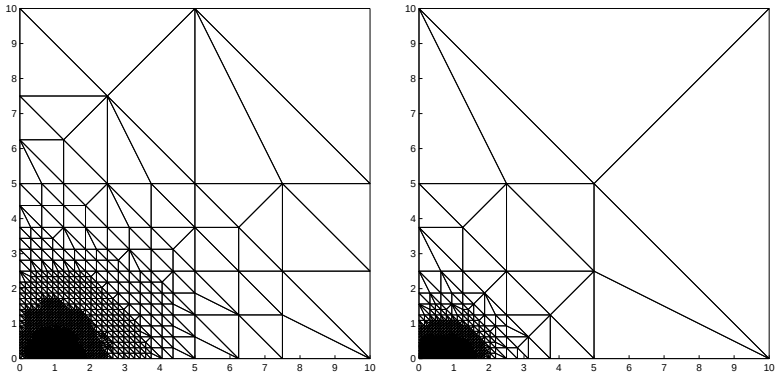

(a) final mesh for $K = 1$, 2665 nodes, 5178 triangles

(b) final mesh for $K = 10$, 2417 nodes, 4682 triangles

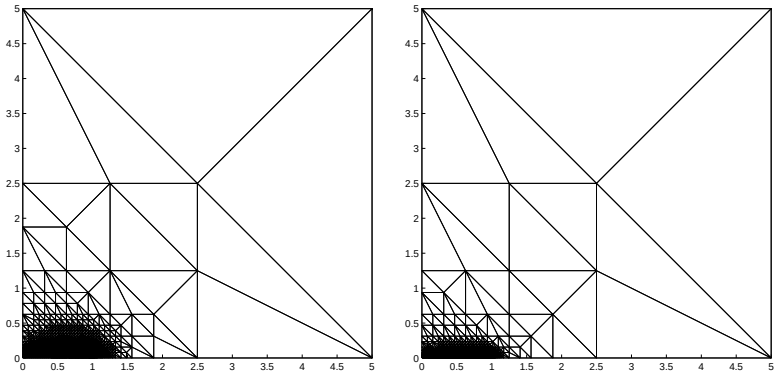

(c) final mesh for $K = 100$, 3452 nodes, 6673 triangles

(d) final mesh for $K = 1000$, 7794 nodes, 15132 triangles

Figure 6: The final meshes for calculating the current to an inlaid microdisc electrode during an EC′ mechanism.

For higher values of K the reaction takes place very close to the electrode surface, and many nodes are required in this region to capture the reaction accurately[2], hence the mesh may remain coarse and uniform further away. The numerical values of the current, error bounds and CPU times are shown in Table 4. Note that the exact solution for $K = 1000$ is computed using Eq. (8.5) and that the Padé approximant Eq. (8.6) given by Rajendran and Sangaranarayanan agrees with the exact solution to 4 decimal places.

[2]In the limit, as K becomes very large, this becomes a one-dimensional problem and would be better solved using 1D methods.

K	adaptive tolerance	exact current	$N_\psi(u^h)$	*a posteriori* error bound	no. of nodes in final mesh	CPU times (secs)
1	0.016	1.6888	1.6871	1.2793×10^{-2}	2665	28.95
10	0.03	3.3223	3.3182	2.8259×10^{-2}	2417	21.76
100	0.08	8.6581	8.6466	7.8708×10^{-2}	3452	23.91
1000	0.25	25.6281	25.6222	0.1487	7794	54.53

Table 4: Steady state current to an inlaid microdisc electrode for different values of K.

10.2 The Recessed Microdisc Electrode

To illustrate our results we consider first the case $L = 0.5$ and again compare with the analytical results for $K = 1$, 10, 100 and 1000. The adaptive tolerance for each case is again chosen to guarantee 1% accuracy in the estimated current. The final mesh for each of the four problems is shown in Figure 7 and again these look as we would expect. As for the inlaid microdisc electrode, for lower K values diffusion is more important and the corner singularity causes more of a problem when evaluating the current, consequently more nodes are needed near the corner. For higher K values the reaction takes place almost entirely within the recess so the mesh may remain coarse further away. These ideas are shown more clearly in Figure 8 which depicts the contours of the solution for each K. It is clear that our completely automated mesh generation algorithm is able to pick out the features in the solution that will have an impact on the simulated current as the governing parameters (in this case K and L) are varied, and refine the mesh appropriately. The numerical values of the current, error bounds and CPU times are shown in Table 5. Agreement is again excellent. We have again achieved much better accuracy than the tolerance that we prescribed, particularly so for $K \gg 1$, since the upper bound Eq. (9.8) overestimates the error to an extent that increases with K. As before, we note that the sharpness of the bound may be improved by avoiding the use of the trace inequality Eq. (A.24).

K	adaptive tolerance	exact current	$N_\psi(u^h)$	*a posteriori* error bound	no. of nodes in final mesh	CPU times (secs)
1	0.01	1.0102	1.0108	9.4585×10^{-3}	745	3.70
10	0.02	2.5095	2.5097	1.3270×10^{-2}	679	2.73
100	0.07	7.8540	7.8540	6.4552×10^{-2}	972	3.78
1000	0.2	24.8365	24.8365	0.1447	3904	14.87

Table 5: Steady state current to a recessed microdisc electrode for $L = 0.5$ and different values of K.

In Figure 9 we show the current for a range of different K and L values, the adaptive tolerance being chosen to give 1% accuracy in the current. Also shown are the approximate analytic values of the current from Eq. (8.12) and Eq. (8.13), and the limiting equation Eq. (8.11); again we note excellent agreement between our numerical approximation and the analytically obtained values.

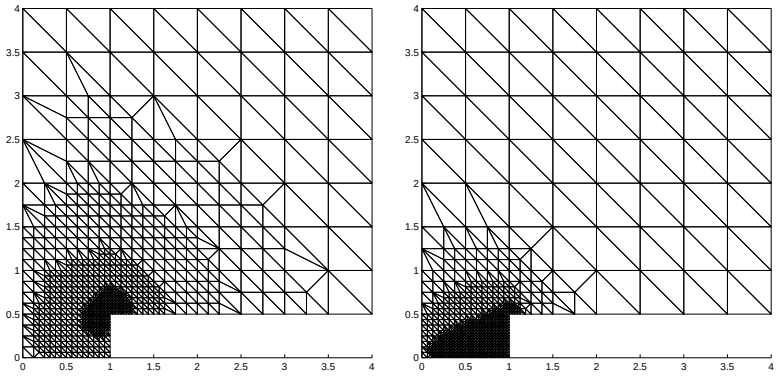

(a) final mesh for $K = 1$, 745 nodes, 1405 triangles

(b) final mesh for $K = 10$, 679 nodes, 1262 triangles

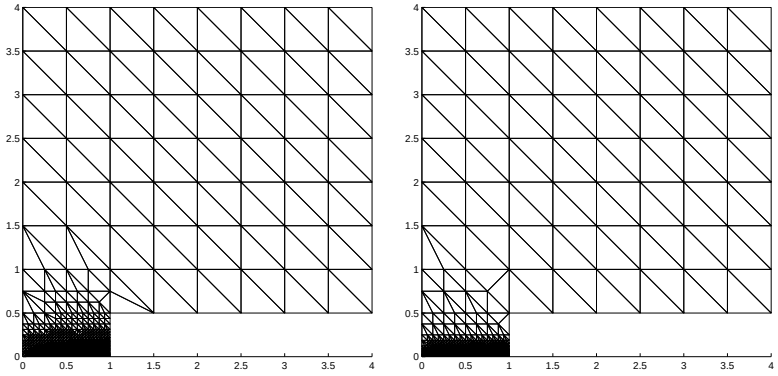

(c) final mesh for $K = 100$, 972 nodes, 1822 triangles

(d) final mesh for $K = 1000$, 3904 nodes, 7494 triangles

Figure 7: The final meshes for calculating the current to a recessed microdisc electrode during an EC$'$ mechanism.

11 Computing

All programs used to generate the results quoted in this paper are written in standard Fortran77 and were run on a Sun Workstation (Sparc Ultra 30) which has a 300MHz processor; in terms of speed this is therefore similar to a mid-range PC with a Pentium II processor.

12 Discussion

In this paper we have described how to derive a mesh refinement algorithm, based on the finite element method, which can be used to calculate the current at a microdisc electrode in the steady state to within a pre-defined tolerance. The algorithm is completely

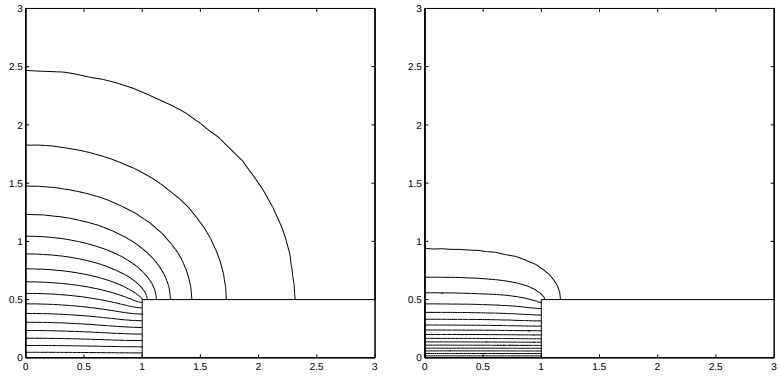

(a) $K = 1$ (b) $K = 10$

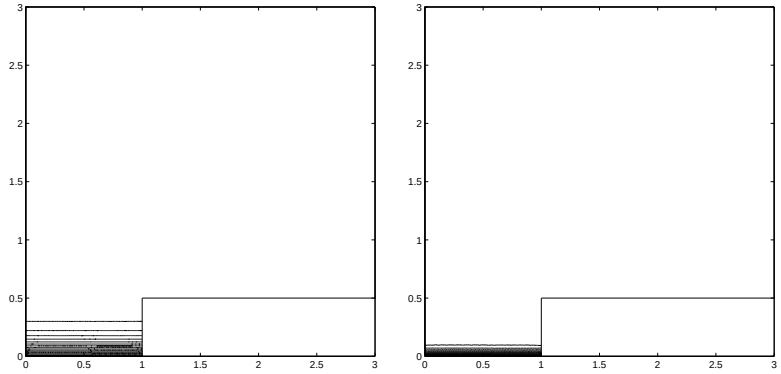

(c) $K = 100$ (d) $K = 1000$

Figure 8: The contours of the solution for different K values. There are 15 equally spaced contours between $u = 0.05$ and $u = 0.95$.

automatic, and requires only that an *a posteriori* bound on the error in the current be derived which is then used to drive the mesh refinement algorithm. In the simple case of an E reaction mechanism the final mesh generated contains only 400 nodes, yet gives an error of only 0.25%.

We have also extended the application of the adaptive finite element method to the more practically relevant cases of a pseudo first-order EC$'$ mechanism at both inlaid and recessed discs. We have been able to demonstrate excellent agreement with recent analytical results [24, 41], confirming the likely accuracy of these results, whilst using minimal computing resources of just a few thousand nodes in our meshes and a few seconds of CPU time on a standard computer. This allows us to highlight the primary advantage of the technique: computation of the simulated current within a *guaranteed* level of accuracy, without the need for excessive computational resources to demonstrate that our codes are numerically convergent. We believe that this method provides an extremely powerful tool for obtaining numerical solutions of electrochemical problems

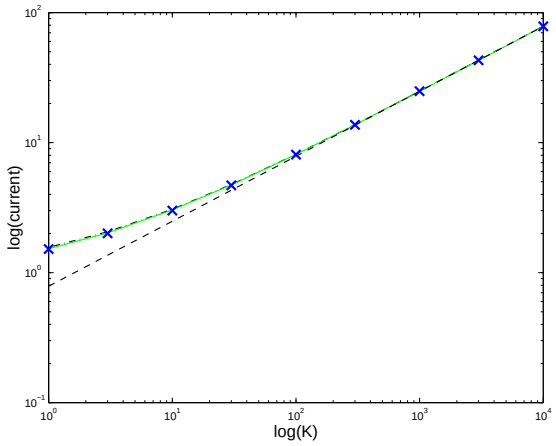

(a) $L = 0.05$

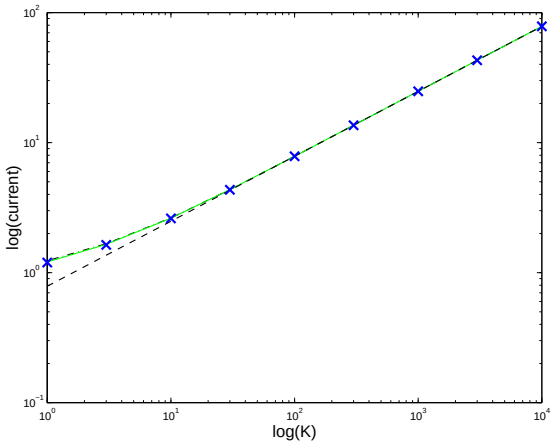

(b) $L = 0.25$

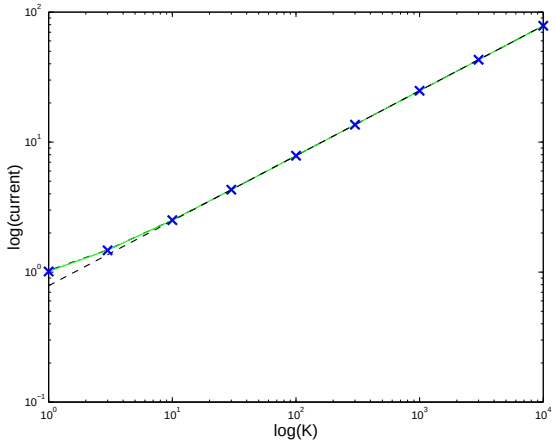

(c) $L = 0.5$

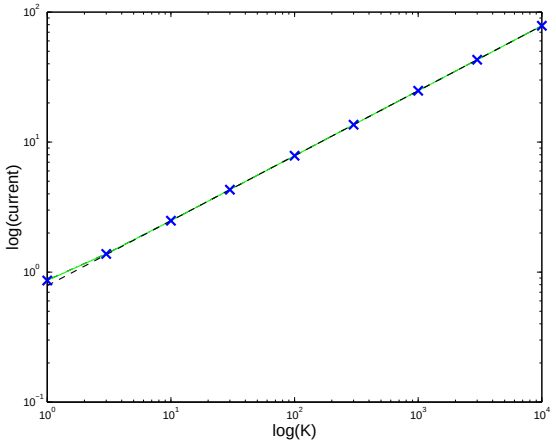

(d) $L = 1$

Figure 9: $\log - \log$ plot of steady state current against K for a range of L values. The key to the graph is: $\times$ finite element simulation, $\cdot - \cdot -$ Eq. (8.12), — Eq. (8.13), $- - -$ Eq. (8.11).

to a guaranteed accuracy for general reaction mechanisms and for general electrode geometries.

We are currently extending this work to time-dependent problems. Our aim is to provide a general algorithm which can be used to obtain the simulated current to within a specified accuracy at any microelectrode geometry, for any reaction mechanism, and for any electrochemical control technique.

13 Acknowledgements

The authors would like to thank Dr Josep Galceran for kindly providing a pre-publication copy of reference [24], and a copy of the associated Mathematica code.

The authors are pleased to acknowledge the financial support of the following organisations: a research studentship from the EPSRC for KH; a Career Development Fellowship from the Medical Research Council for DJG; an EPSRC post-doctoral research grant (GR/K76221) to ES for PH, which has allowed them to undertake this work.

References

[1] J.A. Alden, 1998. *Computational Electrochemistry.* D.Phil thesis, University of Oxford.

[2] J.A. Alden and R.G. Compton, 1997. A General Method for Electrochemical Simulations. 1. Formulation of the Strategy for Two-Dimensional Simulations. *J. Phys. Chem. B*, **101**: 8941.

[3] J.A. Alden and R.G. Compton, 1997. A General Method for Electrochemical Simulations. 2. Application to the Simulation of Steady-State Currents at Microdisk Electrodes: Homogeneous and Heterogeneous Kinetics. *J. Phys. Chem. B*, **101**: 9606.

[4] C.A. Amatore and B. Fosset, 1992. Space variables well fitted for the study of steady state and near steady-state diffusion at a microdisk. *J. Electroanal. Chem.*, **328**: 21.

[5] I. Babuška and A. Miller, 1984. The post-processing approach in the finite element method — Part 1: Calculation of displacements, stresses and other higher derivatives of the displacements. *Int. J. Num. Meth. Engnrg.*, **20**: 1085.

[6] I. Babuška and A. Miller, 1984. The post-processing approach in the finite element method — Part 2: The calculation of stress intensity factors. *Int. J. Num. Meth. Engnrg.*, **20**: 1111.

[7] I. Babuška and A. Miller, 1984. The post-processing approach in the finite element method — Part 3: A posteriori error estimates and adaptive mesh selection. *Int. J. Num. Meth. Engnrg.*, **20**: 2311.

[8] R.E. Bank, 1994. *PLTMG: A Software Package for Solving Elliptic Partial Differential Equations. Users' Guide 7.0.* SIAM.

[9] P.N. Bartlett and S.L. Taylor, 1998. An accurate simulation model for recessed microdisc electrodes. *J. Electroanal. Chem.*, **453**: 49.

[10] R. Becker and R. Rannacher, 1996. A Feedback approach to error control in finite element methods: Basic analysis and examples. *East-West J. Numer. Math.*, **4**: 237.

[11] R. Becker and R. Rannacher, 1998. Weighted a posteriori error control in finite element methods. *In* H.G. Block *et al.*, editor, *ENUMATH-97*, page 621. World Scientific Publishing, Singapore.

[12] A.M. Bond, D. Luscombe, K.B. Oldham and C.G. Zoski, 1988. A comparison of the chronoamperometric response at inlaid and recessed disc microelectrodes. *J. Electroanal. Chem.*, **249**: 1.

[13] S.C. Brenner and L. Ridgeway Scott, 1994. *The Mathematical Theory of Finite Element Methods.* Springer-Verlag.

[14] P.O. Brunn, V.I Fabrikant and T.S. Sankar, 1982. Diffusion through membranes: Effect of a nonzero membrane thickness. *Quart. Journ. Mech. and Applied Math.*, **37**: 311.

[15] J.A. Cooper and R.G. Compton, 1997. Channel Electrodes - A Review. *Electroanalysis*, **10**(3): 141.

[16] J. Crank and R.M. Furzeland, 1977. The Treatment of Boundary Singularities in Axially Symmetric Problems Containing Discs. *J. Inst. Maths. Applics*, **20**: 355.

[17] J.R. Delmastro and D.E. Smith, 1967. An Examination of Some Methods for Obtaining Approximate Solutions to the Expanding-Sphere Boundary Value Problem in Direct Current Polarography. *J. Phys. Chem. B*, **71**: 2138.

[18] G. Denault, M. Fleischmann, D. Pletcher and O.R. Tutty, 1990. Development of the theory for the interpretation of steady state limiting currents at a microelectrode. EC' processes: first and second order reactions. *J. Electroanal. Chem.*, **280**: 243.

[19] I.S. Duff, A.M. Erisman and J.K. Reid, 1997. *Direct Methods for Sparse Matrices.* Clarendon Press.

[20] K. Eriksson, D. Estep, P. Hansbo and C. Johnson, 1995. Introduction to Adaptive Methods for Differential Equations. *In* A. Iserles, editor, *Acta Numerica 1995*, page 105. Cambridge University Press.

[21] K. Eriksson and C. Johnson, 1991. Adaptive Finite Element Methods for Parabolic Problems I: A Linear Model Problem. *SIAM J. Numer. Anal.*, **28**(1): 43.

[22] R. Ferrigno, P.F. Brevet and H.H. Girault, 1997. Finite element simulation of the chronoamperometric response of recessed and protruding microdisc electrodes. *Electrochim. Acta*, **42**: 1895.

[23] J. Galceran, D.J. Gavaghan and J.S. Rollett, 1995. Two-dimensional implementation of the finite element method with singularity correction for diffusion limited current at an unshielded disc electrode. *J. Electroanal. Chem.*, **394**: 17.

[24] J. Galceran, S.L. Taylor and P.N. Bartlett, 1999. Steady State Currents at Inlaid and Recessed Microdisc Electrodes for First-order EC′ Reactions. (in press).

[25] D.J. Gavaghan, 1997. How accurate is your two-dimensional numerical simulation? Part 1. An introduction. *J. Electroanal. Chem.*, **420**: 147.

[26] D.J. Gavaghan, 1998. An exponentially expanding mesh ideally suited to the fast and efficient simulation of diffusion processes at microdisc electrodes. 1. Derivation of the mesh. *J. Electroanal. Chem.*, **456**: 1.

[27] D.J. Gavaghan, 1998. An exponentially expanding mesh ideally suited to the fast and efficient simulation of diffusion processes at microdisc electrodes. 2. Application to chronoamperometry. *J. Electroanal. Chem.*, **456**: 13.

[28] D.J. Gavaghan, 1998. An exponentially expanding mesh ideally suited to the fast and efficient simulation of diffusion processes at microdisc electrodes. 3. Application to voltammetry. *J. Electroanal. Chem.*, **456**: 25.

[29] D.J. Gavaghan and J.S. Rollett, 1990. Correction of boundary singularities in numerical simulation of time-dependent diffusion processes at unshielded disc electrodes. *J. Electroanal. Chem.*, **295**: 1.

[30] I.S. Gradshteyn and I.M. Ryzhik, 1965. *Tables of Integrals, Series and Products.* London Academic Press.

[31] J. Heinze, 1981. Diffusion processes at finite (micro) disk electrodes solved by digital simulation. *J. Electroanal. Chem.*, **124**: 73.

[32] J. Heinze, 1981. Theory of cyclic voltammetry at microdisk electrodes. *Ber. Bunsenges. Phys. Chem.*, **85**: 1096.

[33] P. Houston, 1996. *Lagrange-Galerkin methods for unsteady convection-diffusion problems: a posteriori error analysis and adaptivity.* D.Phil thesis, University of Oxford.

[34] P. Houston, R. Rannacher and E. Süli, 1999. *A posteriori* error analysis for stabilised finite element approximations of transport problems. Technical Report NA99/04, Oxford University Computing Laboratory, Wolfson Building, Parks Road, Oxford OX1 3QD.

[35] C. Johnson, 1987. *Numerical solution of partial differential equations by the finite element method.* Cambridge University Press.

[36] I. Lavagnini, P. Pastore, F. Magno and C.A. Amatore, 1991. Performance of a numerical method based on the hopscotch algorithm and on an oblate spheroidal space coordinate expanding time grid for simulation of voltammetric curves at an inlaid disk microelectrode. *J. Electroanal. Chem.*, **316**: 37.

[37] A.C. Michael, R.M. Wightman and C.A. Amatore, 1989. Microdisk electrodes Part 1. Digital simulation with a conformal map. *J. Electroanal. Chem.*, **267**: 33.

[38] P. Monk and E. Süli, 1998. The adaptive computation of far-field patterns by a posteriori error estimation of linear functionals. *SIAM J. Numer. Anal.*, **36**: 251.

[39] C. Parkins, 1995. *Modelling biosensors: Achieving rapid accuracy for time-dependent currents at disc electrodes.* MSc thesis, University of Oxford.

[40] C.G. Phillips, 1990. The steady, diffusion-limited current at a disc microelectrode with a first order EC′ reaction. *J. Electroanal. Chem.*, **296**: 255.

[41] L. Rajendran and M.V. Sangaranarayanan, 1999. Diffusion at Ultramicro Disk Electrodes: Chronoamperometric Current for Steady-State EC′ Reaction Using Scattering Analogue Techniques. *J. Phys. Chem. B*, **103**: 1518.

[42] J.N. Reddy, 1993. *An Introduction to the Finite Element Method.* McGraw-Hill, 2nd edition.

[43] Y. Saito, 1968. A Theoretical Study on the Diffusion Current at the Stationary Electrodes of Circular and Narrow Band Types. *Rev. Polarogr. (Jpn)*, **15**: 177.

[44] G. Taylor, H.H. Girault and J. McAleer, 1990. Digital-simulation of charge-transfer to an ultramicrodisc interface. *J. Electroanal. Chem.*, **293**: 19.

[45] C.J. Tranter, 1950. On some dual integral equations occuring in potential problems with axial symmetry. *Quart. Journ. Mech. and Applied Math.*, **3**: 411.

[46] C.J. Tranter, 1959. On the analogies between some series containing Bessel functions and certain special cases of the Weber-Schafheitlin integral. *Quart. J. Math. Oxford (2)*, **10**: 110.

[47] M.W. Verbrugge and D.R. Baker, 1992. Transient Diffusion and Migration to a Disk Electrode. *J. Phys. Chem. B*, **96**: 4572.

Appendix A Derivation of the Error Bounds

A.1 The *A Priori* Error Bound for the E Reaction

Consider the error made by the approximation $N_\psi(u^h)$:

$$N_\psi(u) - N_\psi(u^h) \;=\; -\frac{\pi}{2}\int_\Omega \nabla u\cdot\nabla v r dr dz + \frac{\pi}{2}\int_\Omega \nabla u^h\cdot\nabla v^h r dr dz \;. \qquad \text{(A.1)}$$

This holds for all $v \in H^1_\psi(\Omega)$ and $v^h \in S^h_\psi$, so in particular we may make the choice $v = v^h$ to give

$$N_\psi(u) - N_\psi(u^h) \;=\; -\frac{\pi}{2}\int_\Omega \nabla(u-u^h)\cdot\nabla v^h r dr dz \qquad \forall v^h \in S^h_\psi \;. \qquad \text{(A.2)}$$

Now recall from Eq. (3.16) that the dual solution w satisfies

$$B(u-u^h, w) \;=\; 0 \;. \qquad \text{(A.3)}$$

Noting the definition of the bilinear form Eq. (3.9), the identity Eq. (A.3) can be written as

$$\int_\Omega \nabla(u-u^h)\cdot\nabla w r dr dz \;=\; 0 \;. \qquad \text{(A.4)}$$

Combining this with Eq. (A.2) gives

$$N_\psi(u) - N_\psi(u^h) \;=\; -\frac{\pi}{2}\int_\Omega \nabla(u-u^h)\cdot\nabla(v^h-w) r dr dz \qquad \forall v^h \in S^h_\psi \;. \qquad \text{(A.5)}$$

From this identity we can derive an *a priori* error bound. Using the Cauchy-Schwarz inequality [13] on the right-hand side of Eq. (A.5) we see that

$$|N_\psi(u) - N_\psi(u^h)| \;\le\; \frac{\pi}{2} \parallel \nabla(u-u^h) \parallel_{L_2(\Omega)} \parallel \nabla(w-v^h) \parallel_{L_2(\Omega)} \;. \qquad \text{(A.6)}$$

Now we use Céa's lemma (see page 62 of [13]) which states that

$$\parallel \nabla(u-u^h) \parallel_{L_2(\Omega)} \;=\; \inf_{u^*\in S^h_E} \parallel \nabla(u-u^*) \parallel_{L_2(\Omega)} \;, \qquad \text{(A.7)}$$

and so

$$\parallel \nabla(u-u^h) \parallel_{L_2(\Omega)} \;\le\; \parallel \nabla(u-I^h u) \parallel_{L_2(\Omega)} \;, \qquad \text{(A.8)}$$

where $I^h u$ denotes the linear interpolant from S^h_E of u. We also let $v^h = I^h w$, the interpolant from S^h_ψ of w, and use a bound on the interpolation error (see page 104 of [13]) of the form

$$\parallel \nabla(u-I^h u) \parallel \;\le\; C_\epsilon h^{1/2-\epsilon} |u|_{H^{3/2-\epsilon}(\Omega)} \;, \qquad \text{(A.9)}$$

for any $\epsilon \in (0, 1/2)$. Then we have

$$|N_\psi(u) - N_\psi(u^h)| \;\leq\; \tilde{C}_\epsilon h^{1-2\epsilon} \;\;, \tag{A.10}$$

for any $\epsilon \in (0, 1/2)$. The constant $\tilde{C}_\epsilon$ in this *a priori* error bound depends on $|u|_{H^{3/2-\epsilon}(\Omega)}$ and $|w|_{H^{3/2-\epsilon}(\Omega)}$, neither of which are known, so the *a priori* error bound is not computable. Hence, as was indicated earlier, the *a priori* error bound is only useful as an indication of the rate of convergence of the numerical scheme to the true solution of the problem and we see that the error in the computed current is essentially of size $O(h)$. This idea of introducing the dual solution w into the error bound is known as a *duality argument*.

A more useful application of the duality argument will be presented in the next section, to derive a computable *a posteriori* error bound.

A.2 The *A Posteriori* Error Bound for the E Reaction

Consider eliminating u from Eq. (A.5). We know that $v^h \in S^h_\psi$ and $w = \psi$ on $\partial\Omega_D$ so $(v^h - w)|_{\partial\Omega_D} = 0$. Thus the weak formulation Eq. (3.4) of the problem gives

$$\int_\Omega \nabla u \cdot \nabla(v^h - w) r dr dz \;=\; 0 \;\;, \tag{A.11}$$

and we can substitute this into Eq. (A.5) to get

$$N_\psi(u) - N_\psi(u^h) \;=\; \frac{\pi}{2}\int_\Omega \nabla u^h \cdot \nabla(v^h - w) r dr dz \;\;. \tag{A.12}$$

At this point we note that u^h is a piecewise polynomial so ∇u^h exists on Ω but is only piecewise continuous so $\nabla^2 u^h$ may not be meaningful at each point in Ω. However, in the interior of each element α in a triangulation of Ω, $\nabla^2 u^h$ makes sense and is an integrable function so if we write

$$N_\psi(u) - N_\psi(u^h) \;=\; \frac{\pi}{2}\sum_\alpha \int_\alpha \nabla u^h \cdot \nabla(v^h - w) r dr dz \;\;, \tag{A.13}$$

we may apply Green's theorem over each element α to get

$$N_\psi(u) - N_\psi(u^h) \;=\; \frac{\pi}{2}\sum_\alpha \left(\int_\alpha -\nabla^2 u^h \cdot (v^h - w) r dr dz + \int_{\partial\alpha} \frac{\partial u^h}{\partial n}(v^h - w) r ds \right) \tag{A.14}$$

$$= \frac{\pi}{2}\sum_\alpha \int_{\partial\alpha} \frac{\partial u^h}{\partial n}(v^h - w) r ds \;\;, \tag{A.15}$$

since we have chosen u^h to be linear in each triangle α so $\nabla^2 u^h|_\alpha = 0$. Here $\partial\alpha$ denotes the boundary of element α and n is the outward unit normal along $\partial\alpha$.

In this expression v^h, w and r are continuous across element boundaries but $\partial u^h/\partial n$ is not. However, since we have a sum over elements of integrals over their boundaries

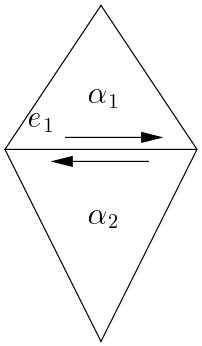

Figure 10: The elements α_1 and α_2.

we can equivalently consider this term to be a sum over all the edges of the elements. Note that since each interior edge is part of two elements there will be two integrals over each interior edge which will not necessarily be the same.

Let us consider a triangulation and, in particular, two elements α_1 and α_2 with common edge e_1 as shown in Figure 10. Then $(v^h - w)$, u^h and r are continuous across e_1 but $\partial u^h/\partial n$ may be discontinuous. Hence the total integral along edge e_1 is

$$\int_{e_1} \left(\frac{\partial u_1^h}{\partial n} - \frac{\partial u_2^h}{\partial n} \right) \left(v^h - w \right) r ds \;=\; \int_{e_1} \left[\frac{\partial u^h}{\partial n} \right] \left(v^h - w \right) r ds \;\;, \tag{A.16}$$

where u_1^h and u_2^h are the expressions for u^h in α_1 and α_2, respectively, and $[\,\cdot\,]$ represents the jump across e_1 so

$$\left[\frac{\partial u^h}{\partial n} \right] \;=\; \lim_{s \to 0} \left(\nabla u^h(\mathbf{r} + s\mathbf{n}_e) - \nabla u^h(\mathbf{r} - s\mathbf{n}_e) \right) \cdot \mathbf{n}_e \;\;, \tag{A.17}$$

where $\mathbf{n}_e$ is the outward unit normal to the edge e of element α. Clearly then we have

$$|N_\psi(u) - N_\psi(u^h)| \;\leq\; \frac{\pi}{2} \sum_e \int_e \left[\frac{\partial u^h}{\partial n} \right] \left(v^h - w \right) r ds \;\;, \tag{A.18}$$

where e are the edges of the elements. Reverting to an integral over $\partial\alpha$ we see that

$$|N_\psi(u) - N_\psi(u^h)| \;\leq\; \frac{\pi}{4} \sum_\alpha \int_{\partial\alpha \setminus \partial\Omega_D} \left| \left[\frac{\partial u^h}{\partial n} \right] \right| |v^h - w| r ds \;\;. \tag{A.19}$$

Note that we have gained a factor of $1/2$ because each edge belongs to two triangles so only half the contribution to each edge contributes to the integral along an edge of any particular triangle. Also the integration is taken over $\partial\alpha \setminus \partial\Omega_D$ only, because $v^h - w = 0$ on $\partial\Omega_D$. Applying the Cauchy Schwarz inequality yields

$$|N_\psi(u) - N_\psi(u^h)| \;\leq\; \frac{\pi}{4} \sum_\alpha \left(\int_{\partial\alpha \setminus \partial\Omega_D} \left| \left[\frac{\partial u^h}{\partial n} \right] \right|^2 r ds \right)^{1/2} \left(\int_{\partial\alpha} |v^h - w|^2 r ds \right)^{1/2} . \tag{A.20}$$

In practice we calculate $\| [\partial u^h/\partial n] \|_{L_2(\partial\alpha)}$ as a sum of the integrals over the three edges of $\triangle_\alpha$ so

$$\int_{\partial\alpha} \left[\frac{\partial u^h}{\partial n}\right]^2 rds = \sum_{i=1}^{3} \int_{e_i} \left[\frac{\partial u^h}{\partial n}\right]^2 rds \quad (A.21)$$

$$= \sum_{i=1}^{3} \int_{e_i} \left(\lim_{s\to 0} \left(\nabla u^h(\mathbf{r}+s\mathbf{n}_e) - \nabla u^h(\mathbf{r}-s\mathbf{n}_e)\right)\cdot \mathbf{n}_e\right)^2 rds \quad (A.22)$$

$$= \sum_{i=1}^{3} \int_{e_i} \left(\left(\nabla u^h(\alpha) - \nabla u^h(\text{neigh}(\alpha,i))\right)\cdot \mathbf{n}_e\right)^2 rds \ , \quad (A.23)$$

where $\nabla u^h(\alpha)$ represents ∇u^h in triangle α and $\nabla u^h(\text{neigh}(\alpha,i))$ represents ∇u^h in the neighbouring triangle which shares edge i with triangle α (e.g. if $\alpha=\alpha_1$ in Figure 10 then $\text{neigh}(\alpha,1)=\alpha_2$). Note that since we are using piecewise linear finite elements for u^h, $\nabla u^h(\alpha)$ and $\nabla u^h(\text{neigh}(\alpha,i))$ are constant which simplifies the integration.

Consider the second term in Eq. (A.20). Let J_α be the transformation matrix defined by Eq. (4.2), then a trace theorem (see page 34 of [13]) can be proved which states that

$$\int_{\partial\alpha} |w|^2 rds \leq \frac{\sqrt{72}}{c_1 h_\alpha^2} \| J_\alpha \|_2 \| w \|_{L_2(\alpha)} \left(\| w \|_{L_2(\alpha)} + \| J_\alpha^T \|_2 \| \nabla w \|_{L_2(\alpha)}\right) \quad (A.24)$$

where h_α is the length of the longest side of triangle α (also known as the diameter of triangle α) and c_1 is a constant dependent on the regularity of the triangle, such that

$$c_1 h_\alpha^2 \leq area(\alpha) \ . \quad (A.25)$$

Note that in cylindrical polar coordinates the norms are weighted so

$$\| w \|_{L_2(\alpha)} = \left(\int_\alpha |w|^2 r dr dz\right)^{1/2} \ . \quad (A.26)$$

The inequality Eq. (A.24) can be used in Eq. (A.20) with $w = v^h - w$ to yield the final *a posteriori* error bound

$$|N_\psi(u) - N_\psi(u^h)| \leq \sum_\alpha \epsilon_\alpha = \epsilon \ , \quad (A.27)$$

where

$$\epsilon_\alpha = \frac{9^{1/4}\pi}{32^{1/4}} \| [\partial u^h/\partial n] \|_{L_2(\partial\alpha)} \frac{\| J_\alpha \|_2^{1/2}}{h_\alpha c_1^{1/2}} \| v^h - w \|_{L_2(\alpha)}^{1/2}$$
$$\times \left(\| v^h - w \|_{L_2(\alpha)} + \| J_\alpha^T \|_2 \| \nabla(v^h - w) \|_{L_2(\alpha)}\right)^{1/2} \ . \quad (A.28)$$

Since w, the exact solution to the dual problem, is not known, we replace w by w^h, the piecewise quadratic finite element approximation to w computed on a triangulation of Ω

which may or may not coincide with the triangulation used to compute u^h. In order to simplify the computation we have chosen to use the same triangulation. We are then free to choose v^h, subject to the constraint $v^h \in S^h_\psi$. Ideally we would like $\| v^h - w^h \|_{L_2(\alpha)}$ and $\| \nabla(v^h - w^h) \|_{L_2(\alpha)}$ to be small so a logical choice of v^h is the linear interpolant of w^h. It is now clear why we needed a higher-order approximation for the dual solution w^h: if we had used piecewise linear finite elements, we would have had $v^h - w^h = 0$ so that our error bound would have been meaningless. We chose the higher-order elements to be piecewise quadratic since this involves the least possible amount of extra work.